PERGAMON

International Journal of Solids and Structures 38 (2001) 8459–8479

INTERNATIONAL JOURNAL OF SOLIDS and STRUCTURES

www.elsevier.com/locate/ijsolstr

Dislocation inside a piezoelectric media with an elliptic inhomogeneity

Zhenyu Huang, Zhen-Bang Kuang *

Department of Engineering Mechanics, School of Civil Engineering, Shanghai Jiaotong University, DongChuan Road 800#, Shanghai 200240, People's Republic of China

Received 23 March 2000

Abstract

In this paper, Green functions for an infinite piezoelectric media with an elliptic piezoelectric inhomogeneity are given for a generalized electro-mechanical force and a generalized electro-mechanical line dislocation that may be located outside, inside or on the interface of elliptic boundary of inhomogeneity. Expressions of Green functions are identical when the generalized force and the generalized dislocation approach to the elliptic boundary from points outside or inside the inhomogeneity. The interaction electric enthalpy between the inhomogeneity and the dislocation is given, which can be used to find the interaction force on the dislocation owing to the existence of the inhomogeneity. Numerical illustrations for the interaction forces are also given and some discussions on the effects of the material mismatches on the interaction forces are made.

Keywords: Piezoelectric; Dislocation; Inhomogeneity; Green function; Stroh formula

1. Introduction

Piezoelectric ceramics are widely used as actuators, sensors and transducers, etc. due to the inherent coupling between their electric and mechanical behavior. Defects such as dislocations, inhomogeneities and cracks inevitably exist in the manufacturing process of materials. When they are subjected to high operating loading and electric voltage, the reliability problem arises in the application of these materials to engineering devices. Therefore it is of great importance to study the electromechanical behavior of piezoelectric materials with defects. Many efforts have been devoted to this field. Deeg (1980) and Pak (1992) analyzed the piezoelectric cracks by a distributed dislocation method. Sosa (1991), Sosa and Khutoryansky (1996) investigated the plane deformation problem of an infinite piezoelectric media with an elliptical void. Wang (1992) conducted an analysis for piezoelectrics with an ellipsoidal inhomogeneity. Chung and Ting (1996) also solved the inclusion problem in piezoelectrics. Researches on the elastic interactions between the dislocation and the inhomogeneity can be found in many papers such as Dundurs and Mura (1964),

* Corresponding author. Tel.: +86-21-54743067; fax: +86-21-62933021.
E-mail addresses: zbkuang@mail.sjtu.edu.cn (Z.-B. Kuang), hzy97025@mail1.sjtu.edu.cn (Z. Huang).

0020-7683/01/$ - see front matter
PII: S0020-7683(01)00062-2

Dundurs and Gangaharan (1969), Warren (1983), Santare and Keer (1986) and Stagni (1995, 1999). Barnett and Lothe (1996) studied the Peach–Koehler image force for a straight dislocation parallel to the interface of two perfectly bonded dissimilar linear elastic half-spaces. They proved that for "proportional" anisotropic bimaterial, i.e. $c^{(1)}_{ijkl} = Kc^{(2)}_{ijkl}$, the dislocation is repelled from the interface when it resides in the elastically softer of the two half-spaces and is attracted to the interface when it resides in the stiffer half-space. The analysis for dislocations in an anisotropic elastic media with an inhomogeneity was elaborated in a series of papers by Hwu and Yen (1993), Yen and Hwu (1994), Yen et al. (1995) and Ting (1996a,b). Recently Deng and Meguid (1998, 1999) conducted an analysis for a screw dislocation in a piezoelectric media. Liang and Hwu (1996), Liu et al. (1997) and Lu and Williams (1998) gave the Green function for a piezoelectric material with an elliptic hole. Pak (1990) studied the force on a piezoelectric screw dislocation. However, to the author's knowledge, the analysis for the interaction of a generalized dislocation interacting with an inhomogeneity in piezoelectric materials has not been reported yet.

The solution of a dislocation inside a piezoelectric media with an inhomogeneity can be served as a kernel function in the distributed dislocation method for solving crack problems. The solution can also be used in the boundary element method as a basic solution function. Furthermore the behavior of dislocations is also of great importance in material science. In Section 2, we will present basic equations. Following Ting's work (1996a,b), in Sections 3 and 5, we give the solutions of an electro-mechanical dislocation that may be located outside, inside the inhomogeneity or on the interface of elliptic boundary of inhomogeneity. The detailed deduction procedure is omitted and the electro-mechanical force is also taken into account. The interaction electric enthalpy between dislocation and inhomogeneity is developed in Section 5. Numerical illustrations for the interaction forces are shown in Section 6 and some discussions on the effects of the material mismatches between the matrix and the inhomogeneity are made. Finally, a conclusion is made for the paper.

2. Basic equations

In a fixed rectangular coordinate system (x_1, x_2, x_3), the constitutive equations for linear piezoelectrics of the second kind can be written as

$$\sigma_{ij} = c_{ijkl}u_{k,l} + e_{lij}\phi_{,l}, \quad D_i = e_{ikl}u_{k,l} - \kappa_{il}\phi_{,l}, \qquad (i,j,k,l = 1,2,3), \tag{1}$$

where repeated Latin indices mean summation and a comma stands for partial differentiation. c_{ijkl} are the elastic stiffnesses under constant electric field, e_{ikl} the piezoelectric constants, and κ_{ij} the permittivity under constant strain field. σ_{ij}, u_i, D_i, ϕ are stress, displacement, electric displacement and electric potential, respectively. Here we only address generalized two-dimensional deformation problem in (x_1, x_2)-plane, i.e. all the variables are constant along the x_3-axis. The poling axis is directed along the x_2-axis. Following Suo et al. (1992), Chung and Ting (1996) and Kuang and Ma (2001) a general displacement solution can be obtained by considering an arbitrary function of linear combination of four complex analytical functions,

$$\mathbf{u} = \begin{Bmatrix} u_j \\ \phi \end{Bmatrix} = 2\,\mathrm{Im}\sum_{\alpha=1}^{4} \mathbf{a}_\alpha f_\alpha(z_\alpha) = 2\,\mathrm{Im}\{\mathbf{A}\langle f(z_\alpha)\rangle\mathbf{q}\}, \tag{2}$$

where $\mathbf{q}$ is an unknown constant vector to be determined. The generalized stress function which is a generalized resultant forces on an arc, can be represented as

$$\mathbf{\Phi}(z) = 2\,\mathrm{Im}\sum_{\alpha=1}^{4} \mathbf{b}_\alpha f_\alpha(z_\alpha) = 2\,\mathrm{Im}\{\mathbf{B}\langle f(z_\alpha)\rangle\mathbf{q}\}, \tag{3}$$

where $z_\alpha = x_1 + p_\alpha x_2$ and $\mathbf{\Phi}_j$, $j = 1, 2, 3$ represent the components of resultant force and $\mathbf{\Phi}_4$ is the electric displacement flux on a curve. In the above $f_\alpha(z_\alpha) = q_\alpha f(z_\alpha)$ is assumed and 'Im' stands for imaginary part. $\mathbf{A}$ and $\mathbf{B}$ are 4×4 complex matrices defined by

$$\mathbf{A} = [\mathbf{a}_1, \mathbf{a}_2, \mathbf{a}_3, \mathbf{a}_4], \quad \mathbf{B} = [\mathbf{b}_1, \mathbf{b}_2, \mathbf{b}_3, \mathbf{b}_4],$$

and $\langle\ \rangle$ stands for a 4×4 diagonal matrix, e.g.

$$\langle f(z_\alpha)\rangle = \mathrm{diag}[f(z_1), f(z_2), f(z_3), f(z_4)].$$

The eigenvalues p_α and eigenvectors $\mathbf{a}_\alpha$ are determined by the following equation:

$$\lfloor \mathbf{Q} + (\mathbf{R} + \mathbf{R}^{\mathrm{T}})p + \mathbf{T}p^2 \rfloor \mathbf{a} = 0, \tag{4}$$

where

$$\mathbf{Q} = \begin{bmatrix} \mathbf{Q}^E & \mathbf{e}_{11} \\ \mathbf{e}_{11}^{\mathrm{T}} & -\kappa_{11} \end{bmatrix}, \quad \mathbf{R} = \begin{bmatrix} \mathbf{R}^E & \mathbf{e}_{21} \\ \mathbf{e}_{21}^{\mathrm{T}} & -\kappa_{12} \end{bmatrix}, \quad \mathbf{T} = \begin{bmatrix} \mathbf{T}^E & \mathbf{e}_{22} \\ \mathbf{e}_{22}^{\mathrm{T}} & -\kappa_{22} \end{bmatrix}, \tag{5}$$

$$Q_{ik}^E = c_{i1k1}, \quad R_{ik}^E = c_{i1k2}, \quad T_{ik}^E = c_{i2k2}, \quad (\mathbf{e}_{ij})_s = e_{ijs},$$

and the eigenvectors $\mathbf{b}_\alpha$ can be obtained from the following relations,

$$\mathbf{b}_\alpha = (\mathbf{R}^{\mathrm{T}} + p_\alpha \mathbf{T})\mathbf{a}_\alpha = -\frac{1}{p_\alpha}(\mathbf{Q} + p_\alpha \mathbf{R})\mathbf{a}_\alpha. \tag{6}$$

The generalized stresses are as follows:

$$\Sigma_{2J}(z) = \begin{Bmatrix} \sigma_{2j} \\ D_2 \end{Bmatrix} = \mathbf{\Phi}_{,1} = 2\,\mathrm{Im}\{\mathbf{B}\langle f'(z_\alpha)\rangle \mathbf{q}\}, \tag{7a}$$

$$\Sigma_{1J}(z) = \begin{Bmatrix} \sigma_{1j} \\ D_1 \end{Bmatrix} = -\mathbf{\Phi}_{,2} = -2\,\mathrm{Im}\{\mathbf{B}\langle p_\alpha f'(z_\alpha)\rangle \mathbf{q}\}. \tag{7b}$$

For stable materials the eigenvalues cannot be real, and here we only consider non-degenerate materials whose eight eigenvalues $p_\alpha, \overline{p}_\alpha$ ($\alpha = 1, 2, 3, 4$) are distinctive. Not losing generality the imaginary part of p_α ($\alpha = 1, 2, 3, 4$) is taken to be positive.

After the normalization for the eigenvectors $\mathbf{A}$ and $\mathbf{B}$, i.e.

$$\mathbf{A}^{\mathrm{T}}\mathbf{B} + \mathbf{B}^{\mathrm{T}}\mathbf{A} = \mathbf{I},$$

the piezoelectric Barnett–Lothe tensors can be written as

$$\mathbf{S} = \mathrm{i}(2\mathbf{A}\mathbf{B}^{\mathrm{T}} - \mathbf{I}), \quad \mathbf{H} = 2\mathrm{i}\mathbf{A}\mathbf{A}^{\mathrm{T}}, \quad \mathbf{L} = -2\mathrm{i}\mathbf{B}\mathbf{B}^{\mathrm{T}}, \tag{8}$$

and the impedance matrix and its inverse are listed as follows:

$$\mathbf{M} = -\mathrm{i}\mathbf{B}\mathbf{A}^{-1} = \mathbf{H}^{-1} + \mathrm{i}\mathbf{H}^{-1}\mathbf{S}, \quad \mathbf{M}^{-1} = \mathrm{i}\mathbf{A}\mathbf{B}^{-1} = \mathbf{L}^{-1} - \mathrm{i}\mathbf{S}\mathbf{L}^{-1}. \tag{9}$$

3. Green function for the dislocation outside the elliptic inhomogeneity

Consider an elliptical piezoelectric inhomogeneity imbedded in an infinite piezoelectric matrix. The inhomogeneity is assumed to be perfectly bonded with the matrix along the interface. The ellipse equation is given by

$$x_1 = a\cos\psi, \quad x_2 = b\sin\psi,$$

where $2a$ and $2b$ are the length of the major and minor axes of the ellipse, respectively, and ψ is a real parameter.

The mapping function

$$z_\alpha = c_\alpha \zeta_\alpha + d_\alpha \zeta_\alpha^{-1}, \tag{10}$$

where

$$c_\alpha = \frac{a - \mathrm{i}p_\alpha b}{2}, \quad d_\alpha = \frac{a + \mathrm{i}p_\alpha b}{2}$$

will transform ellipse into a unit circle. The inverse mapping is taken to be

$$\zeta_\alpha = \frac{z_\alpha + \sqrt{z_\alpha^2 - 4c_\alpha d_\alpha}}{2c_\alpha}. \tag{11}$$

Hwu and Yen (1993) and Ting (1996a,b) pointed out that the mapping is one-to-one for points outside the ellipse in the z_α-plane to points outside the unit circle in the ζ_α-plane. The transformation function maps the interior of the ellipse with a branch cut connecting two points $\tilde{z}_{\alpha 1} = 2\sqrt{c_\alpha d_\alpha}$ and $\tilde{z}_{\alpha 2} = -2\sqrt{c_\alpha d_\alpha}$ in the z_α-plane into the interior of the unit circle with a deprivation of the circle of radius $|\sqrt{t_\alpha}| = |\sqrt{d_\alpha/c_\alpha}|$ in the ζ_α-plane. Detailed discussion on the properties of the mapping function can be consulted from Ting (1996a,b).

Let the generalized line force $\mathbf{f}^*$ and generalized line dislocation $\mathbf{b}^*$ be applied at (x_1^0, x_2^0), where $\mathbf{f}^* = (\mathbf{f}, f_4) = (f_1, f_2, f_3, f_4)$, f_i $(i = 1, 2, 3)$ represents a line force component of $\mathbf{f}$ and f_4 a line charge, $\mathbf{b}^* = (\mathbf{b}, b_4) = (b_1, b_2, b_3, b_4)$, b_i $(i = 1, 2, 3)$ is the component of Burgers vector $\mathbf{b}$ and b_4 represents an electric dipole layer along the slip plane (Barnett and Lothe, 1975). Care should be taken to the discrimination of the half-minor axis b and the Stroh vector $\mathbf{b}_J$, $(J = 1, 2, 3, 4)$ and the Burgers vector $\mathbf{b}$.

Liang and Hwu (1996) stated that without detailed rederivation, the analytical solutions for anisotropic elastic problems can be readily extended to those for piezoelectric materials for two-dimensional problems. So following that of Ting (1996a,b) by extending the sextic Stroh formalism to the octet formalism, the Green function for dislocation outside the inhomogeneity is given as

$$\begin{aligned}\mathbf{\Phi}_1 = {} & \frac{1}{\pi}\mathrm{Im}\left\{\mathbf{B}^{(1)}\left\langle \ln\left(\zeta_\alpha^{(1)} - \zeta_{\alpha 0}^{(1)}\right)\right\rangle \mathbf{q}_1^\infty\right\} + \frac{1}{\pi}\mathrm{Im}\sum_{\beta=1}^{4}\left\{\mathbf{B}^{(1)}\left\langle \ln\left(\zeta_\alpha^{(1)^{-1}} - \overline{\zeta}_{\beta 0}^{(1)}\right)\right\rangle \mathbf{q}_\beta^{(1)}\right\} \\ & + \frac{1}{\pi}\mathrm{Im}\sum_{k=1}^{\infty}\frac{1}{k}\left\{\mathbf{B}^{(1)}\left\langle \left(\zeta_\alpha^{(1)}\right)^{-k}\right\rangle \mathbf{g}_k\right\}\end{aligned} \tag{12}$$

for material 1 outside the inhomogeneity, and

$$\mathbf{\Phi}_2 - \mathbf{\Phi}_2^0 = \frac{1}{\pi}\mathrm{Im}\sum_{\beta=1}^{4}\left\{\mathbf{B}^{(2)}\left\langle \ln\left(z_\alpha^{(2)} - \widehat{z}_{\alpha\beta}^{(2)}\right)\right\rangle \mathbf{q}_\beta^{(2)}\right\} + \frac{1}{\pi}\mathrm{Im}\sum_{k=1}^{\infty}\frac{1}{k}\left\{\mathbf{B}^{(2)}\left\langle f_{k\alpha}^{(2)}\right\rangle \mathbf{h}_k\right\} \tag{13}$$

for material 2 inside the inhomogeneity. The superscripts (1), (2) stand for material 1, 2, respectively. The generalized displacement function $\mathbf{u}_1$ can be obtained when $\mathbf{B}_1$ is replaced by $\mathbf{A}_1$ in Eqs. (12) and (13), so can $\mathbf{u}_2$. In Eqs. (12) and (13)

$$f_{k\alpha}^{(2)} = \left(\zeta_\alpha^{(2)}\right)^k + \left(t_\alpha^{(2)}\right)^k \left(\zeta_\alpha^{(2)}\right)^{-k},$$

$$x_1^0 + p_\alpha^{(1)} x_2^0 = z_{\alpha 0}^{(1)} = c_\alpha^{(1)} \zeta_{\alpha 0}^{(1)} + d_\alpha^{(1)} \left(\zeta_{\alpha 0}^{(1)}\right)^{-1},$$

$$\widehat{x}_1^{\alpha\beta} + p_\alpha^{(2)}\widehat{x}_2^{\alpha\beta} = \widehat{z}_{\alpha\beta}^{(2)} = c_\alpha^{(2)}\zeta_{\beta 0}^{(1)} + d_\alpha^{(2)}\left(\zeta_{\beta 0}^{(1)}\right)^{-1},$$

$\left(\widehat{x}_1^{\alpha\beta}, \widehat{x}_2^{\alpha\beta}\right)$ correspond to sixteen singularities after the mirror image singularities being mapped back to the physical plane for material 2. The sixteen image singularities for material 1 can be found by solving $x_1^{\alpha\beta} + p_\alpha^{(1)}x_2^{\alpha\beta} = z_{\alpha\beta}^{(1)} = c_\alpha^{(1)}\left(\overline{\zeta}_{\beta 0}^{(1)}\right)^{-1} + d_\alpha^{(1)}\overline{\zeta}_{\beta 0}^{(1)}$ for $\left(x_1^{\alpha\beta}, x_2^{\alpha\beta}\right)$. Constant vectors $\mathbf{q}_1^\infty$, $\mathbf{q}_2^\infty$, $\mathbf{q}_\beta^{(1)}$, $\mathbf{q}_\beta^{(2)}$, $\mathbf{g}_k$, $\mathbf{h}_k$, $\mathbf{\Phi}_2^0$, $\mathbf{u}_2^0$ are given in Appendix A. The validity of the solution can be proved by directly substituting Eqs. (12) and (13) into the basic equations.

4. Green function for the dislocation inside the elliptic inhomogeneity and on the elliptic boundary respectively

When the dislocation is located inside the inhomogeneity, analogous to that of Ting (1996a,b), the Green function can be written as

$$\mathbf{\Phi}_1 = \frac{1}{\pi}\mathrm{Im}\left\{\mathbf{B}^{(1)}\left\langle \ln\left(\zeta_\alpha^{(1)} - \zeta_{\alpha 0}^{(2)}\right)\right\rangle \mathbf{q}_1^\infty\right\} + \frac{1}{\pi}\mathrm{Im}\sum_{\beta=1}^{4}\left\{\mathbf{B}^{(1)}\left\langle \ln\left(\zeta_\alpha^{(1)^{-1}} - \zeta_{\beta 0}^{(2)^{-1}}\right)\right\rangle \mathbf{q}_\beta^{(1)}\right\} + \frac{1}{\pi}\mathrm{Im}\sum_{k=1}^{\infty}\frac{1}{k}\left\{\mathbf{B}^{(1)}\left\langle \left(\zeta_\alpha^{(1)}\right)^{-k}\right\rangle \mathbf{g}_k\right\}, \tag{14}$$

$$\mathbf{\Phi}_2 - \mathbf{\Phi}_2^0 = \frac{1}{\pi}\mathrm{Im}\left\{\mathbf{B}^{(2)}\left\langle \ln\left(z_\alpha^{(2)} - z_{\alpha 0}^{(2)}\right)\right\rangle \mathbf{q}_2^\infty\right\} + \frac{1}{\pi}\mathrm{Im}\sum_{\beta=1}^{4}\left\{\mathbf{B}^{(2)}\left\langle \ln\left(z_\alpha^{(2)} - \hat{z}_{\alpha\beta}^{(2)}\right)\right\rangle \left(\mathbf{q}_\beta^{(2)} - \mathbf{I}_\beta\mathbf{q}_2^\infty\right)\right\} + \frac{1}{\pi}\mathrm{Im}\sum_{k=1}^{\infty}\frac{1}{k}\left\{\mathbf{B}^{(2)}\left\langle f_{k\alpha}^{(2)}\right\rangle \mathbf{h}_k\right\}, \tag{15}$$

where

$$x_1^0 + p_\alpha^{(2)}x_2^0 = z_{\alpha 0}^{(2)} = c_\alpha^{(2)}\zeta_{\alpha 0}^{(2)} + d_\alpha^{(2)}\left(\zeta_{\alpha 0}^{(2)}\right)^{-1},$$
$$\hat{x}_1^{\alpha\beta} + p_\alpha^{(2)}\hat{x}_2^{\alpha\beta} = \hat{z}_{\alpha\beta}^{(2)} = c_\alpha^{(2)}\left(\overline{\zeta}_{\beta 0}^{(2)}\right)^{-1} + d_\alpha^{(2)}\overline{\zeta}_{\beta 0}^{(2)}.$$

The $\hat{z}_{\alpha\beta}^{(2)}$ are sixteen image singularities for material 2. The sixteen image singularities for material 1 can be found by solving $\widehat{x}_1^{\alpha\beta} + p_\alpha^{(1)}\widehat{x}_2^{\alpha\beta} = \widehat{z}_{\alpha\beta}^{(1)} = c_\alpha^{(1)}\zeta_{\beta 0}^{(2)} + d_\alpha^{(1)}\left(\zeta_{\beta 0}^{(2)}\right)^{-1}$ for $\left(\widehat{x}_1^{\alpha\beta}, \widehat{x}_2^{\alpha\beta}\right)$. Constant vectors $\mathbf{q}_1^\infty$, $\mathbf{q}_2^\infty$, $\mathbf{q}_\beta^{(1)}$, $\mathbf{q}_\beta^{(2)}$, $\mathbf{g}_k$, $\mathbf{h}_k$, $\mathbf{\Phi}_2^0$, $\mathbf{u}_2^0$ are given in Appendix A.

For the dislocation located on the elliptic boundary

$$x_1^0 = a\cos\psi_0, \quad x_2^0 = b\sin\psi_0,$$

with Eqs. (12) and (13), the Green functions for material 1 and 2, respectively are,

$$\mathbf{\Phi}_1 = \frac{1}{\pi}\mathrm{Im}\left\{\mathbf{B}^{(1)}\left\langle \ln\left(\zeta_\alpha^{(1)} - e^{\mathrm{i}\psi_0}\right)\right\rangle \mathbf{q}_1^\infty\right\} + \frac{1}{\pi}\mathrm{Im}\left\{\mathbf{B}^{(1)}\left\langle \ln\left(\zeta_\alpha^{(1)^{-1}} - e^{-\mathrm{i}\psi_0}\right)\right\rangle \sum_{\beta=1}^{4}\mathbf{q}_\beta^{(1)}\right\} + \frac{1}{\pi}\mathrm{Im}\sum_{k=1}^{\infty}\left\{\frac{1}{k}\mathbf{B}^{(1)}\left\langle \left(\zeta_\alpha^{(1)}\right)^{-k}\right\rangle \mathbf{g}_k\right\}, \tag{16}$$

$$\mathbf{\Phi}_2 - \mathbf{\Phi}_2^0 = \frac{1}{\pi}\mathrm{Im}\left\{\mathbf{B}^{(2)}\left\langle \ln\left(z_\alpha^{(2)} - z_{\alpha 0}^{(2)}\right)\right\rangle \sum_{\beta=1}^{4}\mathbf{q}_\beta^{(2)}\right\} + \frac{1}{\pi}\mathrm{Im}\sum_{k=1}^{\infty}\frac{1}{k}\left\{\mathbf{B}^{(2)}\left\langle f_{k\alpha}^{(2)}\right\rangle \mathbf{h}_k\right\}. \tag{17}$$

Ting (1996a,b) also proved that the limits of the solutions which deduced from the forces and dislocations inside or outside the inhomogeneity are identical with those located on the elliptic boundary for an anisotropic material. The present solution accounts for all the imaginary singularities so it has the same property as that of anisotropic elastic problem. As pointed out by Ting (1996a,b), the solution obtained by Deng and Meguid (1998, 1999) following the lines of Yen and Hwu (1994) and Yen et al. (1995), lost the image singularities, so their solutions may converge slowly or even diverge for points near the missing image singularities when the dislocation approaches the elliptic boundary.

5. Interactions between the dislocation and the inhomogeneity

Following the Eshelby's (1956), the material force can be defined as the negative gradient of the total mechanical and electrical energy with respect to the position change of the defect. In this paper we take the electric enthalpy instead of the internal energy. According to the thermodynamic definition the material force can be deduced as the negative gradient of the electric enthalpy. In the absence of applied electromechanical loading, the total electric enthalpy of the system is equal to the mechanical work plus the electric work required to introduce the dislocation from infinity to the point (x_1^0, x_2^0) where the dislocation is located. In an analogy to Yen and Hwu (1994) and Pak (1990), the total electric enthalpy can be written as

$$H_{\text{tot}} = \frac{1}{2}\int_{x_1^0+\delta}^{\Lambda} (b_i\sigma_{2i} + b_4 D_2)\,\mathrm{d}x_1 \tag{18}$$

where Λ is a large value and δ a small one and their mapping values Λ_α and δ_α still represent large and small values, respectively. When the dislocation is outside the inhomogeneity, noting that Eq. (7a), we get

$$H_{\text{tot}} = \frac{1}{2}\mathbf{b}^{*\mathrm{T}}\mathbf{\Phi}_1\Big|_{z_\alpha^{(1)}=z_{\alpha 0}^{(1)}+\delta_\alpha}^{z_\alpha^{(1)}=\Lambda_\alpha}, \tag{19}$$

where

$$\mathbf{\Phi}_1\Big|_{z_\alpha^{(1)}=z_{\alpha 0}^{(1)}+\delta_\alpha}^{z_\alpha^{(1)}=\Lambda_\alpha} = \frac{1}{\pi}\mathrm{Im}\left\{\mathbf{B}^{(1)}\left\langle \ln\frac{\Lambda_\alpha}{\delta_\alpha}\right\rangle \mathbf{q}_1^\infty + \mathbf{B}^{(1)}\left\langle \ln\left(1-\frac{t_\alpha^{(1)}}{\zeta_{\alpha 0}^{(1)}\zeta_{\alpha 0}^{(1)}}\right)\right\rangle \mathbf{q}_1^\infty - \sum_{\beta=1}^{4}\mathbf{B}^{(1)}\left\langle \ln\left(1-\frac{1}{\zeta_{\alpha 0}^{(1)}\overline{\zeta}_{\beta 0}^{(1)}}\right)\right\rangle \mathbf{q}_\beta^{(1)} - \sum_{k=1}^{\infty}\frac{1}{k}\mathbf{B}^{(1)}\left\langle \zeta_{\alpha 0}^{(1)}\right\rangle^{-k}\mathbf{g}_k\right\}. \tag{20}$$

By excluding the singularities caused by the dislocation, we get the interaction enthalpy for the dislocation located outside the inhomogeneity

$$H_{\text{int}} = \frac{\mathbf{b}^{*\mathrm{T}}}{2\pi}\mathrm{Im}\left\{\mathbf{B}^{(1)}\left\langle \ln\left(1-\frac{t_\alpha^{(1)}}{\zeta_{\alpha 0}^{(1)}\zeta_{\alpha 0}^{(1)}}\right)\right\rangle \mathbf{q}_1^\infty - \sum_{\beta=1}^{4}\mathbf{B}^{(1)}\left\langle \ln\left(1-\frac{1}{\zeta_{\alpha 0}^{(1)}\overline{\zeta}_{\beta 0}^{(1)}}\right)\right\rangle \mathbf{q}_\beta^{(1)} - \sum_{k=1}^{\infty}\frac{1}{k}\mathbf{B}^{(1)}\left\langle \zeta_{\alpha 0}^{(1)}\right\rangle^{-k}\mathbf{g}_k\right\}. \tag{21}$$

When the dislocation is located inside the inhomogeneity, we have

$$H_{\text{tot}} = \frac{1}{2}\mathbf{b}^{*\mathrm{T}}\mathbf{\Phi}_1\Big|_{z_\alpha^{(1)}=z_\alpha^{(1)*}}^{z_\alpha^{(1)}=\Lambda_\alpha} + \frac{1}{2}\mathbf{b}^{*\mathrm{T}}\mathbf{\Phi}_2\Big|_{z_\alpha^{(2)}=z_{\alpha 2}^{(2)}+\delta_\alpha}^{z_\alpha^{(2)}=z_\alpha^{(2)*}}, \tag{22}$$

$$\mathbf{\Phi}_1\Big|_{\substack{z_\alpha^{(1)}=\Lambda_\alpha\\ z_\alpha^{(1)}=z_\alpha^{(1)*}}}+\mathbf{\Phi}_2\Big|_{\substack{z_\alpha^{(2)}=z_\alpha^{(2)*}\\ z_\alpha^{(2)}=z_{\alpha 2}^{(2)}+\delta_\alpha}}=\frac{1}{\pi}\mathrm{Im}\Bigg\{\mathbf{B}^{(1)}\langle\ln\Lambda_\alpha\rangle\mathbf{q}_1^\infty-\mathbf{B}^{(2)}\langle\ln\delta_\alpha\rangle\mathbf{q}_2^\infty-\sum_{k=1}^{\infty}\frac{1}{k}\mathbf{B}^{(2)}\Big\langle f_{k\alpha 0}^{(2)}\Big\rangle\mathbf{h}_k$$
$$-\sum_{\beta=1}^{4}\mathbf{B}^{(2)}\Big\langle\ln\Big(z_{\alpha 0}^{(2)}-\hat{z}_{\alpha\beta}^{(2)}\Big)\Big\rangle\Big(\mathbf{q}_\beta^{(2)}-\mathbf{I}_\beta\mathbf{q}_2^\infty\Big)$$
$$+\sum_{\beta=1}^{4}\ln\Big(-\zeta_{\beta 0}^{(2)}\Big)\Big[-\mathbf{B}^{(1)}\mathbf{q}_\beta^{(1)}+\mathbf{B}^{(2)}\mathbf{I}_\beta\mathbf{q}_2^\infty-\mathbf{B}^{(1)}\mathbf{I}_\beta\mathbf{q}_1^\infty\Big]\Bigg\},$$

$z_\alpha^{(1)*}$, $z_\alpha^{(2)*}$ are the points on the interface and the continuity conditions of the interface are adopted in the above deductions. Just as the manipulations for the dislocation located outside the inhomogeneity, the interaction enthalpy for the dislocation inside the inhomogeneity can be written as

$$H_{\mathrm{int}}=\frac{\mathbf{b}^{*\mathrm{T}}}{2\pi}\mathrm{Im}\Bigg\{-\sum_{k=1}^{\infty}\frac{1}{k}\mathbf{B}^{(2)}\Big\langle f_{k\alpha 0}^{(2)}\Big\rangle\mathbf{h}_k-\sum_{\beta=1}^{4}\mathbf{B}^{(2)}\Big\langle\ln\Big(z_{\alpha 0}^{(2)}-\hat{z}_{\alpha\beta}^{(2)}\Big)\Big\rangle\Big(\mathbf{q}_\beta^{(2)}-\mathbf{I}_\beta\mathbf{q}_2^\infty\Big)$$
$$+\sum_{\beta=1}^{4}\ln\Big(-\zeta_{\beta 0}^{(2)}\Big)\Big[-\mathbf{B}^{(1)}\mathbf{q}_\beta^{(1)}+\mathbf{B}^{(2)}\mathbf{I}_\beta\mathbf{q}_2^\infty-\mathbf{B}^{(1)}\mathbf{I}_\beta\mathbf{q}_1^\infty\Big]\Bigg\}. \tag{23}$$

The generalized interaction force per unit length $\mathbf{F}$ in the $\mathbf{s}$ direction on the dislocation can be written as

$$\mathbf{F}=-\frac{\partial H_{\mathrm{int}}}{\partial\mathbf{s}}, \tag{24}$$

which is very complicated and a numerical calculation will be conducted in the next section.

6. Numerical examples and discussions

In this section the solutions obtained in the foregoing sections are used to find the interaction forces applied to the dislocation due to the existence of the inhomogeneity. The aspect ratio of the ellipse is 1/3 for all numerical examples. We first give the contour plots of the glide and climb forces for the dislocation located inside the PZT-5H matrix with an epoxy, an isolating void and a rigid conductor inhomogeneity, respectively. Then we will investigate the effect of different elastic, piezoelectric and dielectric mismatches on the interaction forces, respectively.

6.1. Contour plots of the interaction forces for practical engineering material pairs

In available literatures, material constants are measured in the material coordinate system (X_1, X_2, X_3) where the poling axis is X_3. In this coordinate system, material constants for PZT-5H and epoxy, which are taken to be the first material pair, are listed as follows:

PZT-5H matrix (Kuo and Huang, 1997):

$$c_{11}^{(1)}=126\ \mathrm{GPa},\ c_{33}^{(1)}=117\ \mathrm{GPa},\ c_{44}^{(1)}=35.3\ \mathrm{GPa},\ c_{12}^{(1)}=55\ \mathrm{GPa},\ c_{13}^{(1)}=53\ \mathrm{GPa},$$
$$e_{31}^{(1)}=-6.5\ \mathrm{cm}^{-2},\ e_{33}^{(1)}=23.3\ \mathrm{cm}^{-2},\ e_{15}^{(1)}=17.0\ \mathrm{cm}^{-2},\ \kappa_{11}^{(1)}=15.1\times10^{-9}\ \mathrm{C}^2\mathrm{N}^{-1}\mathrm{m}^{-2},$$
$$\kappa_{33}^{(1)}=13.0\times10^{-9}\ \mathrm{C}^2\mathrm{N}^{-1}\mathrm{m}^{-2}.$$

Epoxy inhomogeneity (Dunn and Taya, 1993):

$$c_{11}^{(2)} = 6.43 \text{ GPa},\ c_{33}^{(2)} = 6.429 \text{ GPa},\ c_{44}^{(2)} = 1.07 \text{ GPa},\ c_{12}^{(2)} = 4.29 \text{ GPa},\ c_{13}^{(2)} = 4.289 \text{ GPa},$$
$$e_{31}^{(2)} = e_{33}^{(2)} = e_{15}^{(2)} = 0 \text{ cm}^{-2},\ \kappa_{11}^{(2)} = 5.0 \times 10^{-9} \text{ C}^2\text{N}^{-1}\text{m}^{-2},\ \kappa_{33}^{(2)} = 5.001 \times 10^{-9} \text{ C}^2\text{N}^{-1}\text{m}^{-2}.$$

For epoxy material constants, small perturbations have been performed to avoid repeated eigenvalues. Since in Section 2 we take the poling axis to be along the x_2-axis, the corresponding relationship between (X_1, X_2, X_3) and (x_1, x_2, x_3) is

$$X_3 \to x_2, \quad X_1 \to x_1, \quad X_2 \to x_3.$$

Hence the matrices **Q**, **R**, **T** defined in Eq. (5) for a transversely isotropic piezoelectric material are as follows:

$$\mathbf{Q} = \begin{bmatrix} c_{11} & 0 & 0 & 0 \\ 0 & c_{44} & 0 & e_{15} \\ 0 & 0 & \frac{c_{11}-c_{12}}{2} & 0 \\ 0 & e_{15} & 0 & -\kappa_{11} \end{bmatrix}, \quad \mathbf{R} = \begin{bmatrix} 0 & c_{13} & 0 & e_{31} \\ c_{44} & 0 & 0 & 0 \\ 0 & 0 & 0 & 0 \\ e_{15} & 0 & 0 & 0 \end{bmatrix}, \quad \mathbf{T} = \begin{bmatrix} c_{44} & 0 & 0 & 0 \\ 0 & c_{33} & 0 & e_{33} \\ 0 & 0 & c_{44} & 0 \\ 0 & e_{33} & 0 & -\kappa_{33} \end{bmatrix},$$

where the material constants are measured in the (X_1, X_2, X_3) coordinate system.

We suppose an imaginary inhomogeneity whose material constants are proportional to those of the matrix, i.e.

$$K = \frac{c_{ijkl}^{(2)}}{c_{ijkl}^{(1)}} = \frac{e_{lij}^{(2)}}{e_{lij}^{(1)}} = \frac{\kappa_{ij}^{(2)}}{\kappa_{ij}^{(1)}}. \tag{25}$$

By letting $K \to 0$ and $K \to \infty$, the material pairs can be used to simulate a matrix containing an isolating void and a conducting rigid inhomogeneity respectively. In our program the ratios are taken to be $K = 0.001$ and $K = 1000$, respectively, which are taken to be the second and the third material pairs.

From dimensional analysis, L_{11} in Eq. (8) has a dimension of N/m^2, and we choose the non-dimensionalized factor to be $L_{11} \times 10^{-9}\ \text{m}/4\pi$ for the interaction forces. In our calculation, the electric dislocation (ED) and the mechanical dislocation (MD) are assumed to be located at the same position. Three cases are considered, i.e. $b_1 = 2b$, $b_4 = 0$; $b_1 = 0$, $b_4 = 2b \times 10^9$ V/m and $b_1 = 2b$, $b_4 = 2b \times 10^9$ V/m while all the other dislocation components are supposed to be zero. To the authors' knowledge, there are no numerical solutions for interaction forces for a piezoelectric dislocation interacted with an inhomogeneity. Therefore the correctness of the routine programmed by the authors was verified by comparing the results by Yen and Hwu (1994) for an anisotropic media without electric components. The influence of the interaction forces caused by the ED on the MD is obtained by the assumption that the ED moves along with the MD. In the present text, moving directions of the dislocation are presumed to be along the x_1-axis and the x_2-axis. Hence from Eq. (24) the dimensionless glide force applied on the dislocation along the slip direction ox_1 and the dimensionless climb force along the direction ox_2 can be written as

$$F_1 = -\frac{4\pi \partial H_{\text{int}}}{L_{11}\,\partial x_1} \times 10^9, \quad F_2 = -\frac{4\pi \partial H_{\text{int}}}{L_{11}\,\partial x_2} \times 10^9. \tag{26}$$

Decompose F_1 and F_2 into three terms, i.e. terms containing b_1^2 , b_4^2 and $b_1 b_4$, respectively,

$$F_1 = F_{111}\left(b_1^2\right) + F_{144}\left(b_4^2\right) + F_{114}(b_1 b_4), \quad F_2 = F_{211}\left(b_1^2\right) + F_{244}\left(b_4^2\right) + F_{214}(b_1 b_4). \tag{27}$$

The interaction forces $F_{111}(b_1^2)$ and $F_{211}(b_1^2)$ are produced by the MD only, $F_{144}(b_4^2)$ and $F_{244}(b_4^2)$ by the ED only, and $F_{114}(b_1 b_4)$ and $F_{214}(b_1 b_4)$ are the coupling terms between the MD and the ED. F_{111} and F_{211} are even functions of b_1 and F_{144} and F_{244} is even function of b_4. The sign change of b_1 and b_4 will influence the coupling terms F_{114} and F_{214}, but not F_{111}, F_{144}, F_{211} and F_{244}.

In all plots the positive interaction glide forces denote that the dislocation is repelled from the x_2-axis; the negative ones denote that the dislocation is attracted to the x_2-axis. The foregoing statement also applies to the interaction climb forces once the x_2-axis is replaced by the x_1-axis. In all numerical results, the glide force F_1 is zero when the dislocation is on the x_2-axis and the climb force F_2 is zero when the dislocation is on the x_1-axis, which can be explained by the symmetry of the material properties and the geometric configuration. The position where F_1 is zero is an equilibrium one for the glide forces and it is the same case for the climb forces when $F_2 = 0$. The stability of the equilibrium is determined by the attraction or repulsion condition around the equilibrium position. For example, in Figs. 1a and 4a, the x_2-axis is a stable equilibrium position for the glide component of the interaction forces; in Figs 1b and 4b the x_1-axis is a stable equilibrium position for the climb component of the interaction forces. The ED either enhances or weakens the interaction between the inhomogeneity and the MD depending on the mismatch of the material pairs and the position where the dislocation located. In all contour plots, when the MD or the ED approaches the inhomogeneity, the absolute value of interaction forces increases. When the dislocation is away from the inhomogeneity, the absolute value decreases which means that the influence of the inhomogeneity diminishes.

Figs. 1–9 show the contour diagrams for an epoxy inhomogeneity, an isolating void and a rigid conductor, respectively. Comparing Figs. 1–3 and Figs. 4–6, it is seen that the contour plots for an isolating

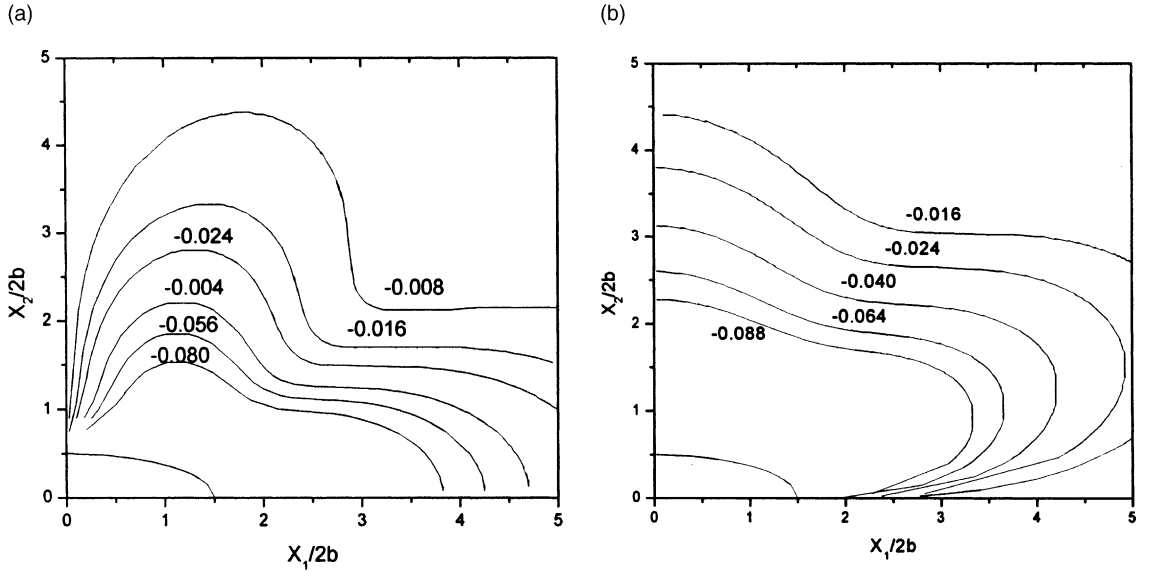

Fig. 1. (a) Contour plots of the dimensionless glide force F_1 for PZT-5H matrix containing an epoxy inhomogeneity with $\mathbf{b}^*/2b = \{1,0,0,0\}$. (b) Contour plots of the dimensionless climb force F_2 for PZT-5H matrix containing an epoxy inhomogeneity with $\mathbf{b}^*/2b = \{1,0,0,0\}$.

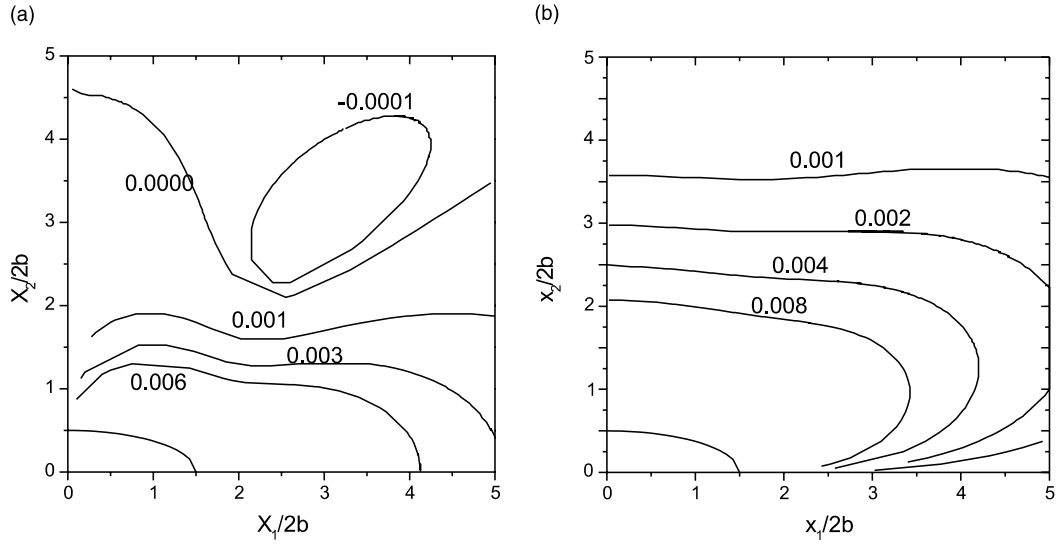

Fig. 2. (a) Contour plots of the dimensionless glide force F_1 for PZT-5H matrix containing an epoxy inhomogeneity with $\mathbf{b}^*/2b = \{0, 0, 0, 10^9\}$. (b) Contour plots of the dimensionless climb force F_2 for PZT-5H matrix containing an epoxy inhomogeneity with $\mathbf{b}^*/2b = \{0, 0, 0, 10^9\}$.

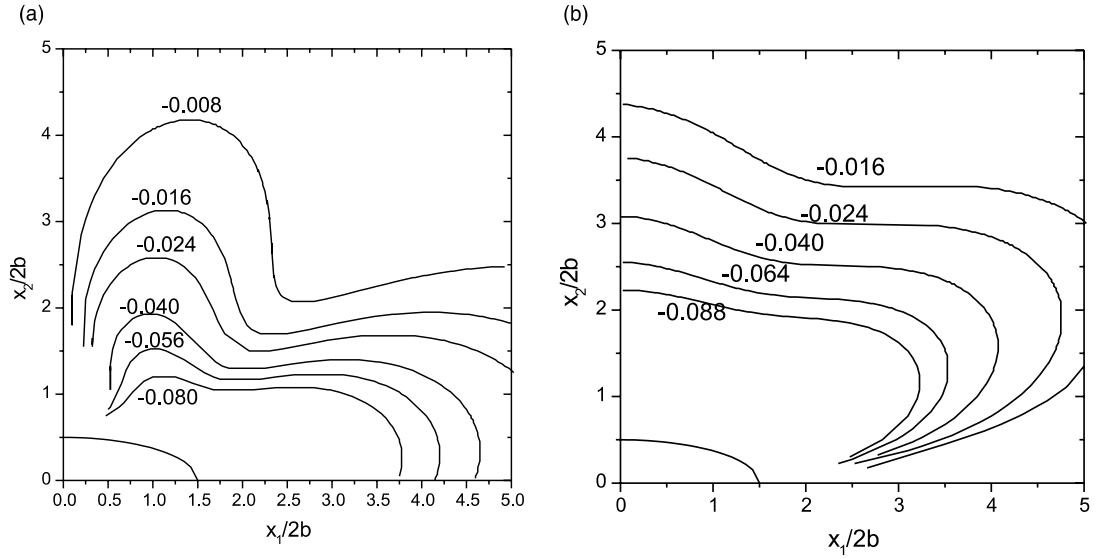

Fig. 3. (a) Contour plots of the dimensionless glide force F_1 for PZT-5H matrix containing an epoxy inhomogeneity with $\mathbf{b}^*/2b = \{1, 0, 0, 10^9\}$. (b) Contour plots of the dimensionless climb force F_2 for PZT-5H matrix containing an epoxy inhomogeneity with $\mathbf{b}^*/2b = \{1, 0, 0, 10^9\}$.

void differ a little from those for an epoxy and the influence by an isolating void on the interaction forces is a little greater than that by an epoxy inhomogeneity. It can also be observed that the interaction forces

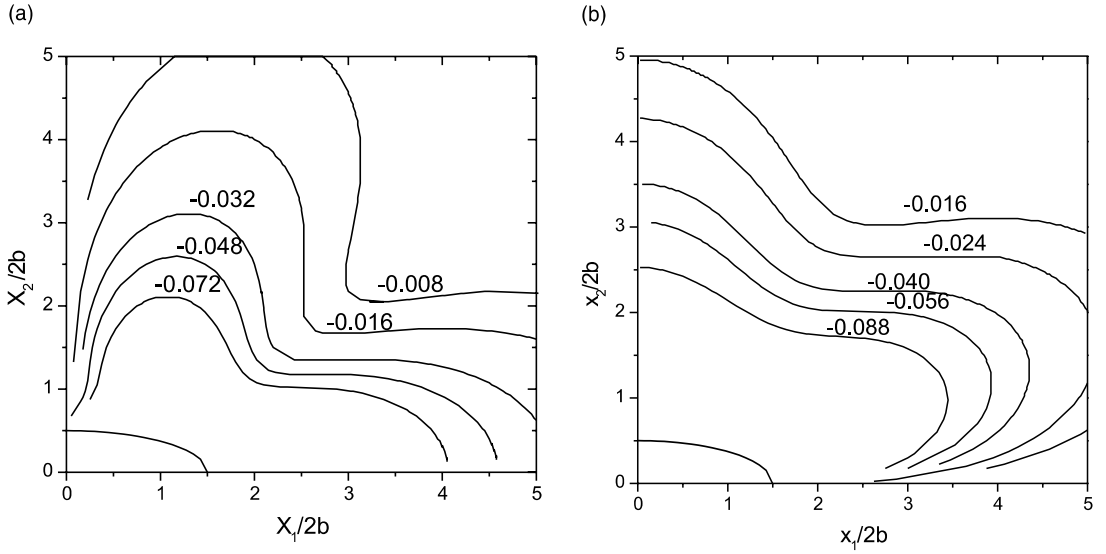

Fig. 4. (a) Contour plots of the dimensionless glide force F_1 for PZT-5H matrix containing an isolating void with $\mathbf{b}^*/2b = \{1, 0, 0, 0\}$. (b) Contour plots of the dimensionless climb force F_2 for PZT-5H matrix containing an isolating void with $\mathbf{b}^*/2b = \{1, 0, 0, 0\}$.

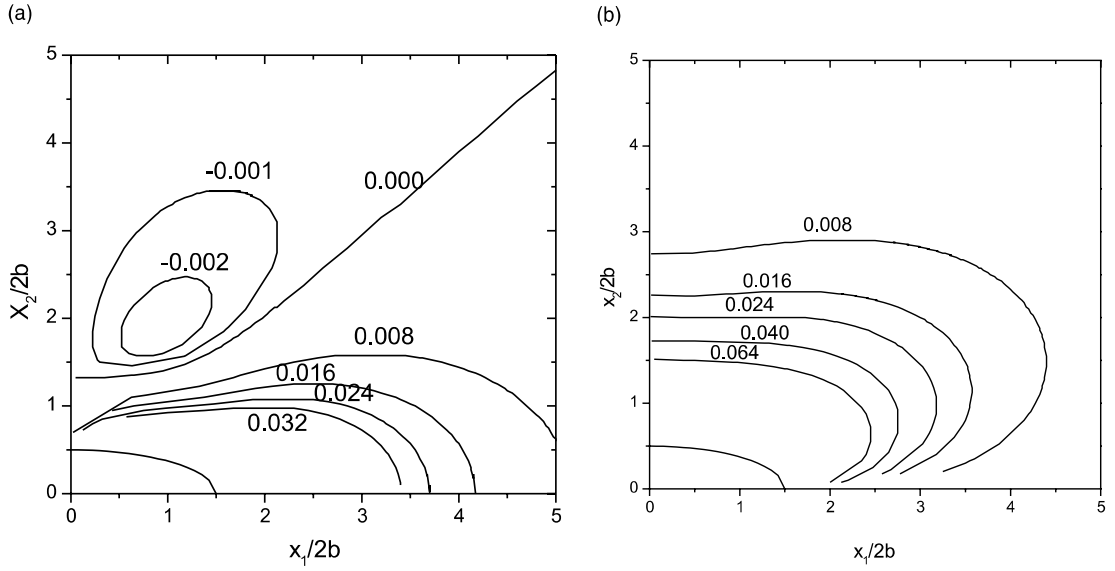

Fig. 5. (a) Contour plots of the dimensionless glide force F_1 for PZT-5H matrix containing an isolating void with $\mathbf{b}^*/2b = \{0, 0, 0, 10^9\}$. (b) Contour plots of the dimensionless climb force F_2 for PZT-5H matrix containing an isolating void with $\mathbf{b}^*/2b = \{0, 0, 0, 10^9\}$.

caused by the ED on the MD is small for both the isolating and the epoxy inhomogeneity. However, for the rigid conductor (Figs. 7–9) the ED significantly alters the interaction forces of the MD especially for the

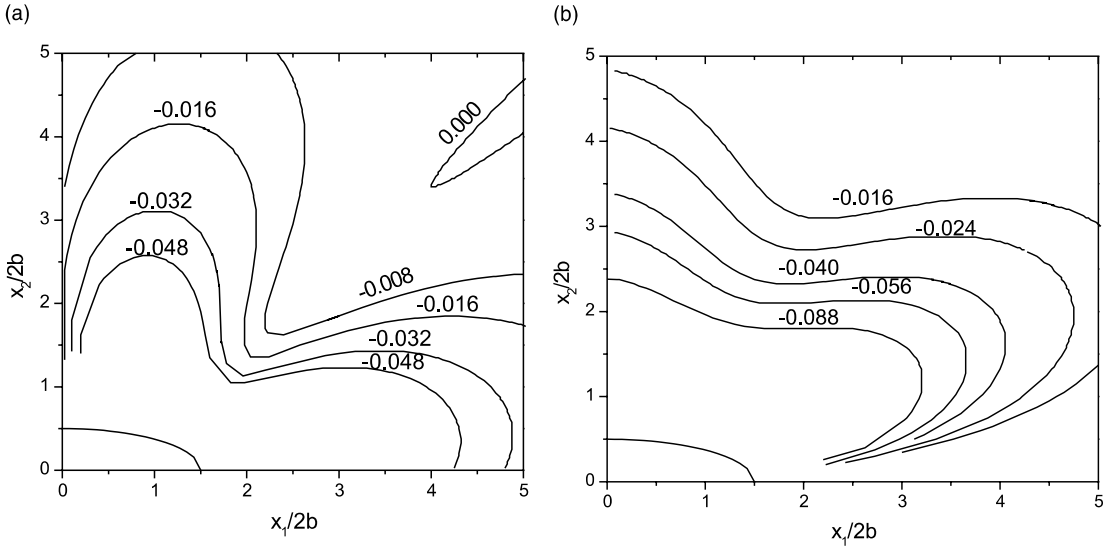

Fig. 6. (a) Contour plots of the dimensionless glide force F_1 for PZT-5H matrix containing an isolating void with $\mathbf{b}^*/2b = \{1, 0, 0, 10^9\}$. (b) Contour plots of the dimensionless climb force F_2 for PZT-5H matrix containing an isolating void with $\mathbf{b}^*/2b = \{1, 0, 0, 10^9\}$.

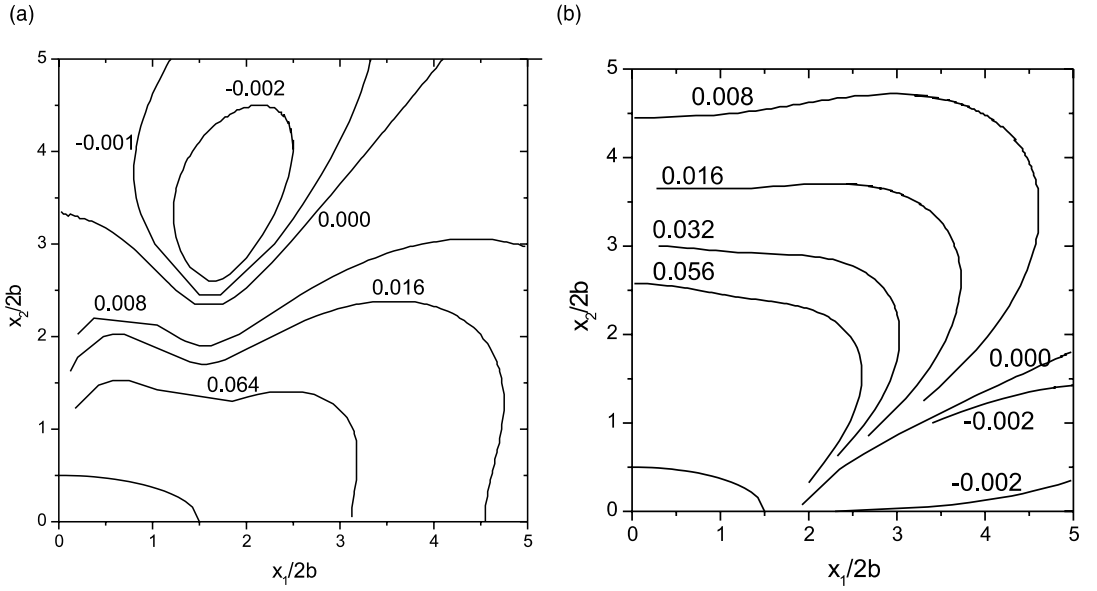

Fig. 7. (a) Contour plots of the dimensionless glide force F_1 for PZT-5H matrix containing a rigid conductor with $\mathbf{b}^*/2b = \{1, 0, 0, 0\}$. (b) Contour plots of the dimensionless climb force F_2 for PZT-5H matrix containing a rigid conductor with $\mathbf{b}^*/2b = \{1, 0, 0, 0\}$.

climb forces (Fig. 9). In the plotted region of Figs. 1 and 4, the interaction forces are all negative which means the inhomogeneity always tends to attract the MD. If there exists an ED only, the glide interaction

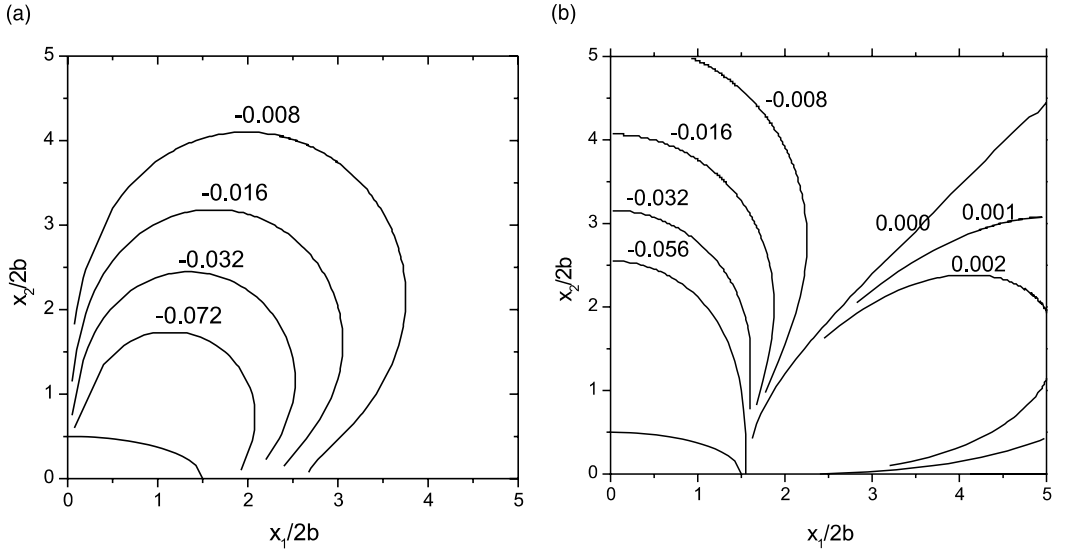

Fig. 8. (a) Contour plots of the dimensionless glide force F_1 for PZT-5H matrix containing a rigid conductor with $\mathbf{b}^*/2b = \{0, 0, 0, 10^9\}$. (b) Contour plots of the dimensionless climb force F_2 for PZT-5H matrix containing a rigid conductor with $\mathbf{b}^*/2b = \{0, 0, 0, 10^9\}$.

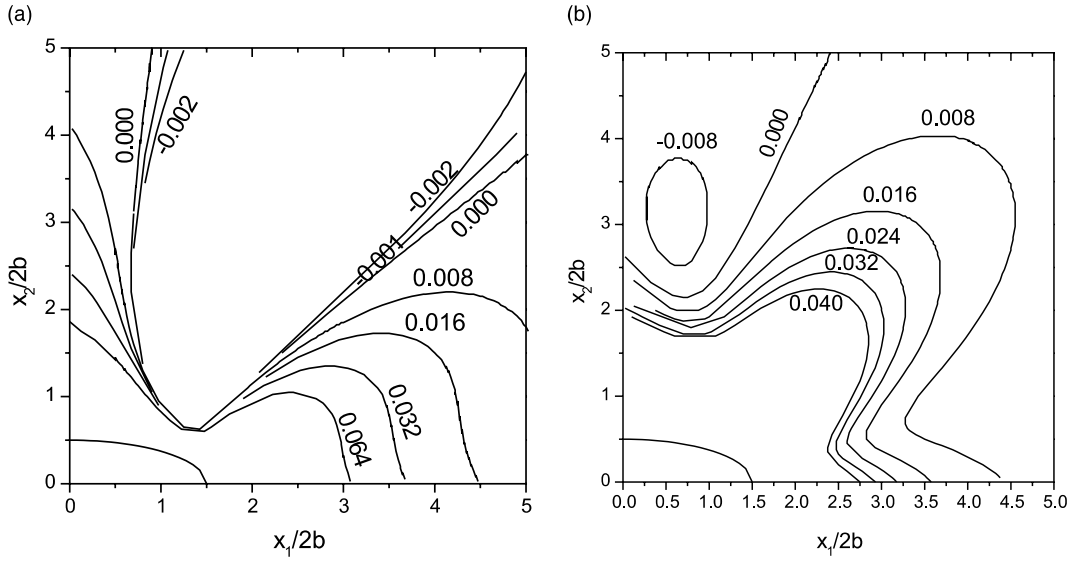

Fig. 9. (a) Contour plots of the dimensionless glide force F_1 for PZT-5H matrix containing a rigid conductor with $\mathbf{b}^*/2b = \{1, 0, 0, 10^9\}$. (b) Contour plots of the dimensionless climb force F_2 for PZT-5H matrix containing a rigid conductor with $\mathbf{b}^*/2b = \{1, 0, 0, 10^9\}$.

forces may be positive or negative depending the position of the ED (Figs. 2a and 5a) and the climb forces are positive (Figs. 2b and 5b), which means that the ED may be repelled or attracted by the x_2-axis and it is always repelled by the x_1-axis in this case.

6.2. Investigation of the influences of the material mismatches on the interaction forces

The above subsection is devoted to the material pairs in practical engineering applications. To investigate the effect of the elastic, piezoelectric and dielectric mismatches on the interaction forces, respectively, we define three material constant ratios namely the elastic, piezoelectric and dielectric ratio,

$$k_{\mathrm{e}} = \frac{c^{(2)}_{ijkl}}{c^{(1)}_{ijkl}}, \quad k_{\mathrm{p}} = \frac{e^{(2)}_{lij}}{e^{(1)}_{lij}}, \quad k_{\mathrm{d}} = \frac{\kappa^{(2)}_{ij}}{\kappa^{(1)}_{ij}}.$$

If $k_{\mathrm{e}} > 1$, $k_{\mathrm{p}} > 1$ and $k_{\mathrm{d}} > 1$, respectively, we say, the inhomogeneity is elastically, piezoelectrically and dielectrically harder than the matrix, otherwise, softer. In the following computation, by varying one of the mismatch ratios while keeping the other two equal to 1, we can investigate the interaction forces with respect to the variations of the above mismatch constants, respectively. Here the interaction forces are plotted for the dislocation located both inside and outside the inhomogeneity. Figs. 10a–16a show the glide forces when the dislocation is on the x_1-axis and Figs. 10b–16b show the climb forces when it on the x_2-axis. From Figs. 10–16, the interaction forces on the dislocation can be closely observed when it passes through the interface along the coordinate axes. When the MD is near the interface, the interaction forces approach infinite. This is due to the simplification of a singular dislocation in a elastic continuum involving a sharp change in the material constants (Dundurs and Gangaharan, 1969). The interaction forces are zero at the origin (at the center of the elliptical inhomogeneity). When the dislocation is inside the inhomogeneity, generally, the absolute value of the interaction forces monotonously increases as the dislocation approaching the interface (except Fig. 14). When the dislocation is outside the inhomogeneity, the absolute value of the interaction forces monotonously decreases as the dislocation leaving the interface. The interaction force approaches zero when the dislocation is far away from the inhomogeneity.

6.2.1. Case for a single MD only (Figs. 10–12)

For the case that there is no ED and exists a single MD only, we can observe from Fig. 10 that the higher the elastic mismatch ratio, the larger the interaction forces. It is the same for the piezoelectric mismatch ratio (Fig. 11) but opposite for the dielectric mismatch ratio (Fig. 12).

(I) $k_{\mathrm{e}} < 1, \quad k_{\mathrm{p}} < 1, \quad k_{\mathrm{d}} > 1.$

It can be observed from Figs. 10–12 that the MD is attracted by the x_1-axis and the x_2-axis no matter the MD is located inside or outside the inhomogeneity, which suggest that the elastically, piezoelectrically softer and dielectrically harder inhomogeneity attracts the MD.

When the MD is located inside the inhomogeneity, the curves of the interaction forces for the different material constant ratios are almost indiscernible (Figs. 10–12). It is suggested that the effect of material mismatch on the interaction forces is small for the single MD located inside the inhomogeneity. However, when the MD is located outside the inhomogeneity, the mismatch effect is obvious.

(II) $k_{\mathrm{e}} > 1, \quad k_{\mathrm{p}} > 1, \quad k_{\mathrm{d}} < 1.$

The MD is repelled by the x_1-axis and the x_2-axis for the elastically, piezoelectrically harder and dielectrically softer inhomogeneity respectively. When the MD is located inside or outside the inhomogeneity, the mismatch effect is significant.

6.2.2. Case for an ED coexisting with a MD (Figs. 13–15)

When the ED coexists with the MD, the interaction forces for the dislocation inside the inhomogeneity vary greatly for the elastic mismatch (Fig. 13) compared to those for the MD alone (Fig. 10). For the elastic and dielectric mismatch, the ED cannot significantly influence the interaction forces caused by the MD,

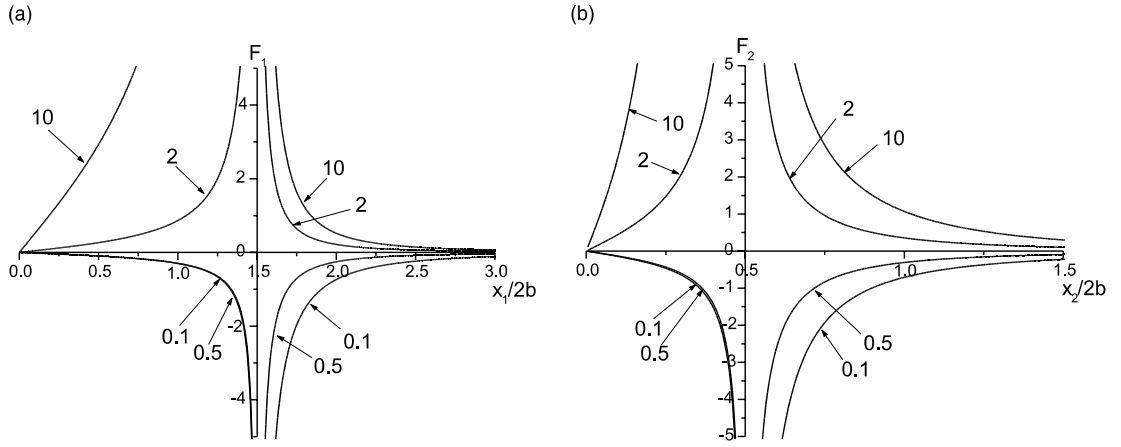

Fig. 10. (a) Variations of the dimensionless glide force F_1 with respect to different elastic mismatch ratios k_e for the dislocation on the x_1-axis with Burgers vector $\mathbf{b}^*/2b = \{1, 0, 0, 0\}$. (b) Variations of the dimensionless climb force F_2 with respect to different elastic mismatch ratios k_e for the dislocation on the x_2-axis with Burgers vector $\mathbf{b}^*/2b = \{1, 0, 0, 0\}$.

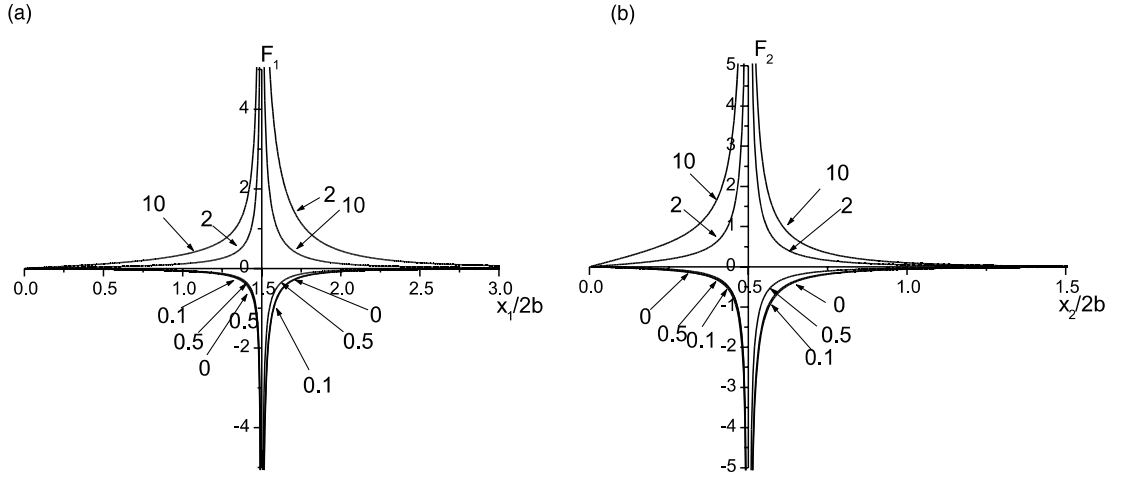

Fig. 11. (a) Variations of the dimensionless glide force F_1 with respect to different piezoelectric mismatch ratios k_p for the dislocation on the x_1-axis with Burgers vector $\mathbf{b}^*/2b = \{1, 0, 0, 0\}$. (b) Variations of the dimensionless climb force F_2 with respect to different piezoelectric mismatch ratios k_p for the dislocation on the x_2-axis with Burgers vector $\mathbf{b}^*/2b = \{1, 0, 0, 0\}$.

except the case $k_e < 1$, $k_d > 1$ and the dislocation is located inside the inhomogeneity (viz. except the regions of the third quadrant in Figs. 13 and 15).

It can be seen that the piezoelectric mismatch effect is more profound than the elastic mismatch and dielectric mismatch effects (Fig. 14), the sign of the interaction glide and climb forces for $k_p = 10$ and $k_p = 2$ (Fig. 14) are totally reversed compared to those of Fig. 11. There exists an unstable equilibrium position for the glide force for $k_p = 10$ and $k_p = 2$ when the dislocation located outside the inhomogeneity (Fig. 14a); an stable equilibrium position for the interaction climb forces exists for the dislocation inside the

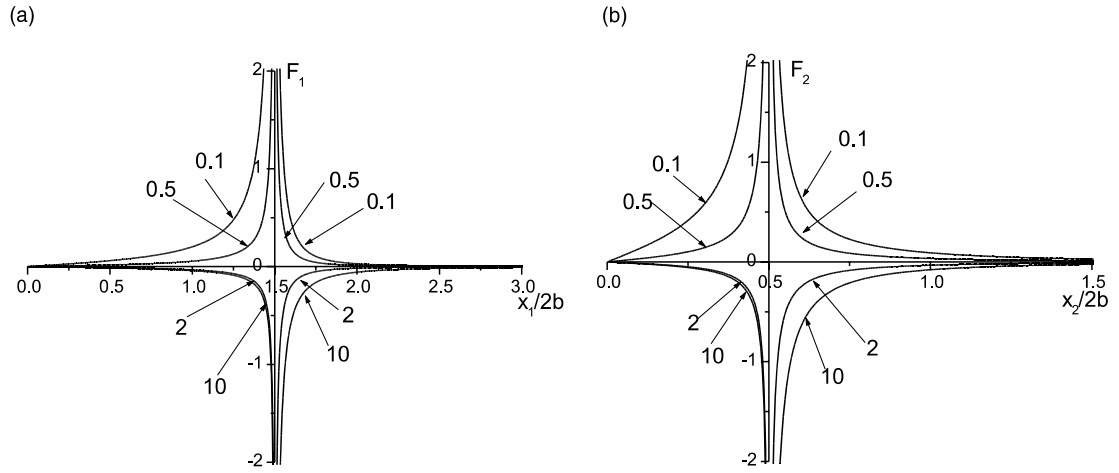

Fig. 12. (a) Variations of the dimensionless glide force F_1 with respect to different dielectric mismatch ratios k_d for the dislocation on the x_1-axis with Burgers vector $\mathbf{b}^*/2b = \{1, 0, 0, 0\}$. (b) Variations of the dimensionless climb force F_2 with respect to different dielectric mismatch ratios k_d for the dislocation on the x_2-axis with Burgers vector $\mathbf{b}^*/2b = \{1, 0, 0, 0\}$.

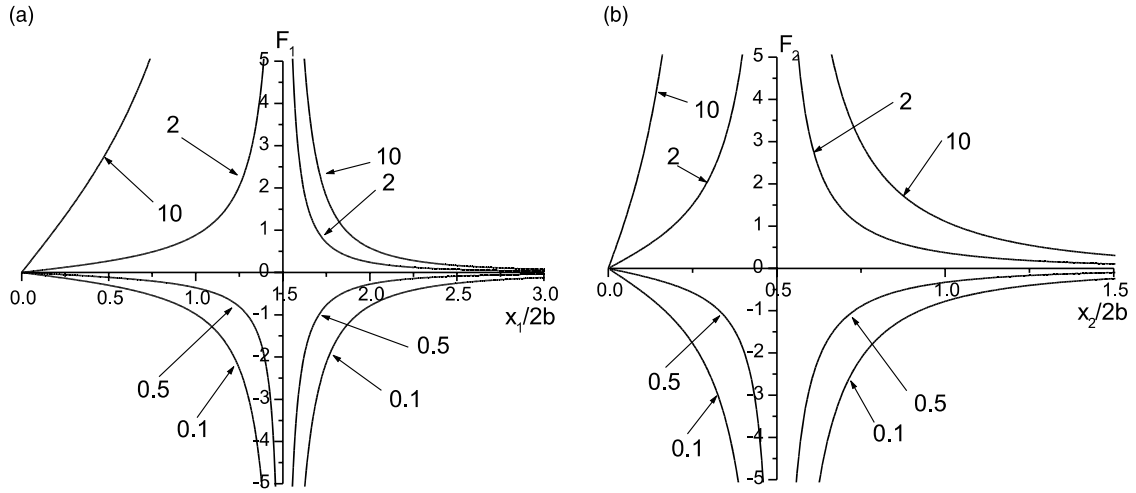

Fig. 13. (a) Variations of the dimensionless glide force F_1 with respect to different elastic mismatch ratios k_e for the dislocation on the x_1-axis with Burgers vector $\mathbf{b}^*/2b = \{1, 0, 0, 10^9\}$. (b) Variations of the dimensionless climb force F_2 with respect to different elastic mismatch ratios k_e for the dislocation on the x_2-axis with Burgers vector $\mathbf{b}^*/2b = \{1, 0, 0, 10^9\}$.

inhomogeneity for $k_p = 0.1$ and $k_p = 0$ (Fig. 14b). The piezoelectric mismatch effect is not large for the dislocation located outside the inhomogeneity for $k_p < 1$ (Fig. 14). The interaction forces by a single ED for different piezoelectric mismatches (Fig. 16) are supplied to illustrate its effect on the MD. For $k_p > 1$, the interaction forces are negative (Fig. 16) which are positive in Fig. 11; for $k_p < 1$, the interaction forces are positive (Fig. 16) which are negative in Fig. 11. Therefore, the equilibrium position in Fig. 14 may be

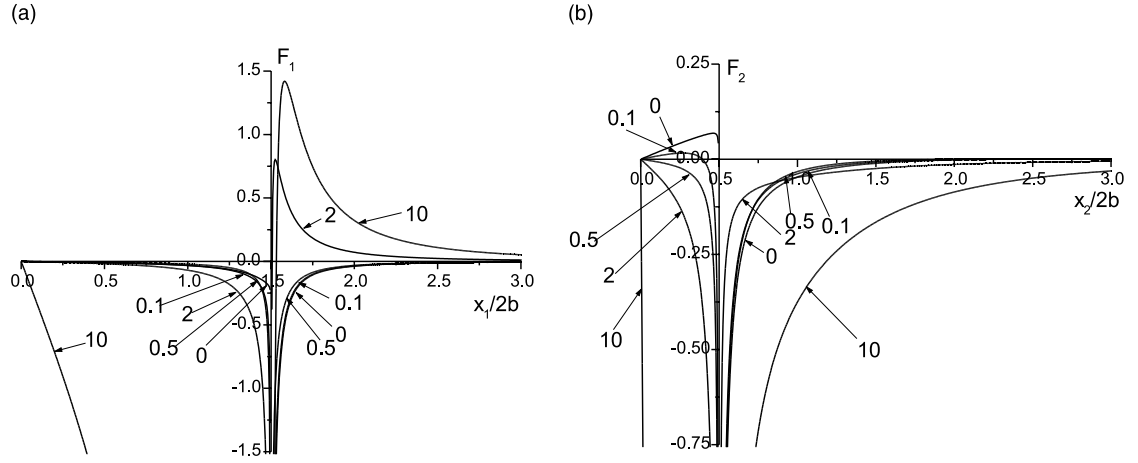

Fig. 14. (a) Variations of the dimensionless glide force F_1 with respect to different piezoelectric mismatch ratios k_p for the dislocation on the x_1-axis with Burgers vector $\mathbf{b}^*/2b = \{1, 0, 0, 10^9\}$. (b) Variations of the dimensionless climb force F_2 with respect to different piezoelectric mismatch ratios k_p for the dislocation on the x_2-axis with Burgers vector $\mathbf{b}^*/2b = \{1, 0, 0, 10^9\}$.

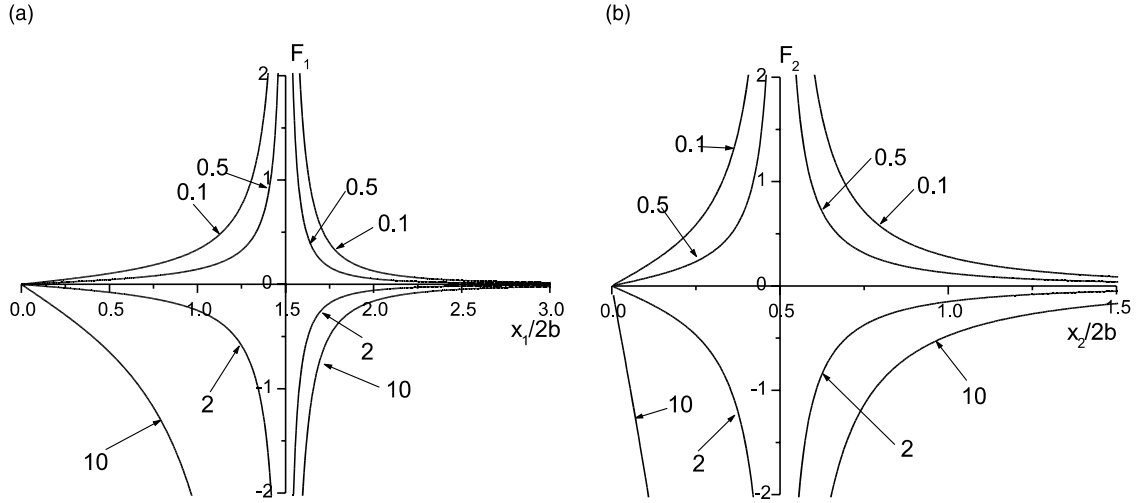

Fig. 15. (a) Variations of the dimensionless glide force F_1 with respect to different dielectric mismatch ratios k_d for the dislocation on the x_1-axis with Burgers vector $\mathbf{b}^*/2b = \{1, 0, 0, 10^9\}$. (b) Variations of the dimensionless climb force F_2 with respect to different dielectric mismatch ratios k_d for the dislocation on the x_2-axis with Burgers vector $\mathbf{b}^*/2b = \{1, 0, 0, 10^9\}$.

explained by the cancellation of the interaction forces caused by the MD (Fig. 11) and the ED (Fig. 16) and their coupling effects between the MD and the ED. These piezoelectric mismatch plots suggest that when the inhomogeneity is piezoelectrically harder and the elastic and dielectric properties of the matrix and inhomogeneity are approximately the same, the piezoelectric mismatch may significantly change the interaction forces even the attribute of them when the ED coexists with the MD.

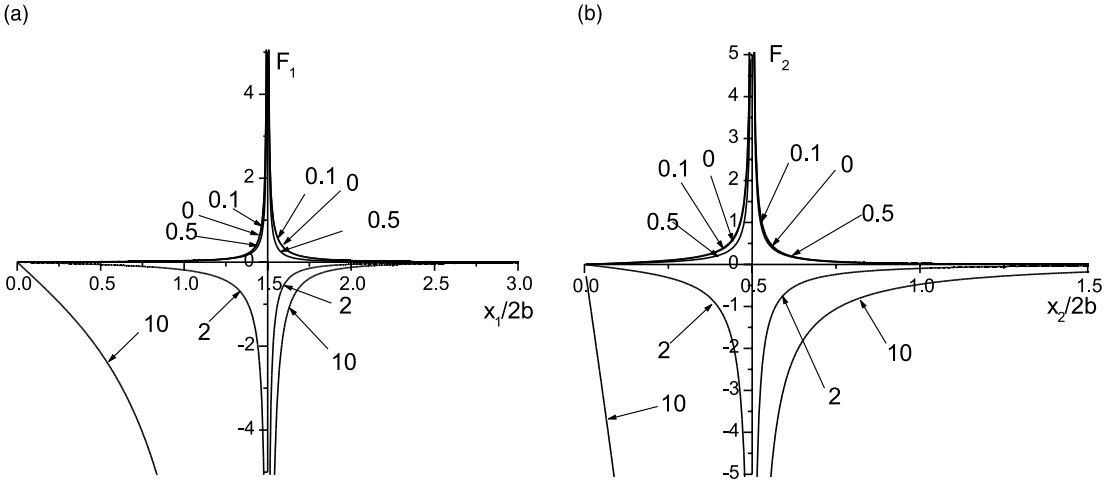

Fig. 16. (a) Variations of the dimensionless glide force F_1 with respect to different piezoelectric mismatch ratios k_p for the dislocation on the x_1-axis with Burgers vector $\mathbf{b}^*/2b = \{0, 0, 0, 10^9\}$. (b) Variations of the dimensionless climb force F_2 with respect to different piezoelectric mismatch ratios k_p for the dislocation on the x_2-axis with Burgers vector $\mathbf{b}^*/2b = \{0, 0, 0, 10^9\}$.

7. Conclusions

In this paper, Green functions for an infinite piezoelectric media with an elliptic piezoelectric inhomogeneity are given for an electro-mechanical force and electro-mechanical line dislocation that may be located outside, inside the inhomogeneity or on the interface of elliptic boundary of inhomogeneity. Expressions of Green functions are identical when the generalized force and the generalized dislocation approach to the elliptic boundary from points outside or inside the inhomogeneity. The interaction electric enthalpy between inhomogeneity and dislocation is given, which can be used to find the forces on the dislocation owing to existence of the inhomogeneity. Numerical illustrations and discussions for the interaction forces are given. The results manifest that the electric dislocation can increase or decrease the interaction forces between the mechanical dislocation and inhomogeneity depending on the position of the dislocation. The mismatch of the material properties and the position of the dislocation significantly influence the interaction forces. It is found that the mismatch effect on the interaction forces is not significant for certain cases.

Acknowledgements

This work is supported by the national science foundation of China through the Grant 10072033. Helpful suggestions by the reviewers are gratefully acknowledged.

Appendix A

$$\mathbf{q}_1^{\infty} = \mathbf{A}^{(1)^{\mathrm{T}}}\mathbf{f}^* + \mathbf{B}^{(1)^{\mathrm{T}}}\mathbf{b}^*, \quad \mathbf{q}_2^{\infty} = \mathbf{A}^{(2)^{\mathrm{T}}}\mathbf{f}^* + \mathbf{B}^{(2)^{\mathrm{T}}}\mathbf{b}^*,$$

$$\mathbf{I}_1 = \mathrm{diag}[1, 0, 0, 0], \quad \mathbf{I}_2 = \mathrm{diag}[0, 1, 0, 0], \quad \mathbf{I}_3 = \mathrm{diag}[0, 0, 1, 0], \quad \mathbf{I}_4 = \mathrm{diag}[0, 0, 0, 1],$$

$$\mathbf{X}=\mathbf{I}+\frac{1}{2}\mathbf{L}^{(2)}\left(\mathbf{M}^{(1)^{-1}}-\mathbf{M}^{(2)^{-1}}\right)=\frac{1}{2}\mathbf{L}^{(2)}\left(\mathbf{M}^{(1)^{-1}}+\overline{\mathbf{M}}^{(2)^{-1}}\right),$$

$$\mathbf{Y}_k=\mathbf{B}^{(2)}\left\langle\left(t_\alpha^{(2)}\right)^k\right\rangle\mathbf{B}^{(2)^{\mathrm{T}}}\left(\overline{\mathbf{M}}^{(1)^{-1}}-\overline{\mathbf{M}}^{(2)^{-1}}\right),$$

$$\mathbf{g}_k=\mathbf{B}^{(1)^{-1}}\left(\mathbf{X}-\mathbf{Y}_k\overline{\mathbf{X}}^{-1}\overline{\mathbf{Y}}_k\right)^{-1}\left(\mathrm{i}\mathbf{Y}_k\overline{\mathbf{X}}^{-1}\overline{\mathbf{y}}_k-\mathbf{y}_k\right),$$

$$\mathbf{h}_k=\mathrm{i}\mathbf{B}^{(2)^{\mathrm{T}}}\left(\overline{\mathbf{M}}^{(2)^{-1}}-\overline{\mathbf{M}}^{(1)^{-1}}\right)\left(\overline{\mathbf{B}}^{(1)}\overline{\mathbf{g}}_k\right),$$

where $\mathbf{Y}_k$ and $\mathbf{y}_k$ are given in the following for case 1 and case 2.

Case 1: Constant vectors for the dislocation outside the inhomogeneity

$$\mathbf{q}_\beta^{(1)}=\mathbf{B}^{(1)^{-1}}\left(\mathbf{M}^{(1)^{-1}}+\overline{\mathbf{M}}^{(2)^{-1}}\right)^{-1}\left(\overline{\mathbf{M}}^{(2)^{-1}}-\overline{\mathbf{M}}^{(1)^{-1}}\right)\overline{\mathbf{B}}^{(1)}\mathbf{I}_\beta\overline{\mathbf{q}}_1^{\infty},$$

$$\mathbf{q}_\beta^{(2)}=\mathbf{B}^{(2)^{-1}}\left(\overline{\mathbf{M}}^{(1)^{-1}}+\mathbf{M}^{(2)^{-1}}\right)^{-1}\left(\mathbf{M}^{(1)^{-1}}+\overline{\mathbf{M}}^{(1)^{-1}}\right)\mathbf{B}^{(1)}\mathbf{I}_\beta\mathbf{q}_1^{\infty},$$

$$\mathbf{y}_k=\sum_{\beta=1}^{4}\mathbf{B}^{(2)}\left\langle\left(\widehat{\tau}_{\alpha\beta}^{(2)}\right)^k\right\rangle\mathbf{q}_\beta^{(2)},\quad \widehat{\tau}_{\alpha\beta}^{(2)}=t_\alpha^{(2)}\zeta_{\beta0}^{(1)^{-1}},$$

$$\mathbf{u}_2^0=-\frac{1}{\pi}\mathrm{Im}\left\{\mathbf{A}^{(2)}\left\langle\ln c_\alpha^{(2)}\right\rangle\mathbf{q}^{(2)}\right\},\quad \mathbf{\Phi}_2^0=-\frac{1}{\pi}\mathrm{Im}\left\{\mathbf{B}^{(2)}\left\langle\ln c_\alpha^{(2)}\right\rangle\mathbf{q}^{(2)}\right\},\quad \mathbf{q}^{(2)}=\sum_{\beta=1}^{4}\mathbf{q}_\beta^{(2)}.$$

Case 2: Constant vectors for the dislocation inside the inhomogeneity

$$\begin{aligned}\mathbf{q}_\beta^{(1)}=\mathbf{B}^{(1)^{-1}}&\left(\mathbf{M}^{(1)^{-1}}+\overline{\mathbf{M}}^{(2)^{-1}}\right)^{-1}\left\{\left(\overline{\mathbf{M}}^{(2)^{-1}}-\overline{\mathbf{M}}^{(1)^{-1}}\right)\overline{\mathbf{B}}^{(1)}\mathbf{I}_\beta\overline{\mathbf{q}}_1^{\infty}+2\overline{\mathbf{M}}^{(2)^{-1}}\,\mathrm{Re}\left[\mathbf{B}^{(2)}\mathbf{I}_\beta\mathbf{q}_2^{\infty}-\mathbf{B}^{(1)}\mathbf{I}_\beta\mathbf{q}_1^{\infty}\right]\right.\\&\left.+2\mathrm{iRe}\left[\mathbf{A}^{(2)}\mathbf{I}_\beta\mathbf{q}_2^{\infty}-\mathbf{A}^{(1)}\mathbf{I}_\beta\mathbf{q}_1^{\infty}\right]\right\},\end{aligned}$$

$$\begin{aligned}\mathbf{q}_\beta^{(2)}=\mathbf{B}^{(2)^{-1}}&\left(\overline{\mathbf{M}}^{(1)^{-1}}+\mathbf{M}^{(2)^{-1}}\right)^{-1}\left\{\left(\mathbf{M}^{(1)^{-1}}+\overline{\mathbf{M}}^{(1)^{-1}}\right)\mathbf{B}^{(1)}\mathbf{I}_\beta\mathbf{q}_1^{\infty}+2\overline{\mathbf{M}}^{(1)^{-1}}\,\mathrm{Re}\left[\mathbf{B}^{(2)}\mathbf{I}_\beta\mathbf{q}_2^{\infty}-\mathbf{B}^{(1)}\mathbf{I}_\beta\mathbf{q}_1^{\infty}\right]\right.\\&\left.+2i\mathrm{Re}\left[\mathbf{A}^{(2)}\mathbf{I}_\beta\mathbf{q}_2^{\infty}-\mathbf{A}^{(1)}\mathbf{I}_\beta\mathbf{q}_1^{\infty}\right]\right\},\end{aligned}$$

$$\mathbf{u}_2^0=-\frac{1}{\pi}\mathrm{Im}\sum_{\beta=1}^{4}\left\{\mathbf{A}^{(2)}\left\langle\ln c_\alpha^{(2)}\right\rangle\mathbf{q}_\beta^{(2)}+\ln\left(-\zeta_{\beta0}^{(2)}\right)\left[\mathbf{A}^{(2)}\mathbf{I}_\beta\mathbf{q}_2^{\infty}-\mathbf{A}^{(1)}\mathbf{I}_\beta\mathbf{q}_1^{\infty}\right]\right\},$$

$$\mathbf{\Phi}_2^0 = -\frac{1}{\pi}\mathrm{Im}\sum_{\beta=1}^{4}\left\{\mathbf{B}^{(2)}\left\langle \ln c_\alpha^{(2)}\right\rangle \mathbf{q}_\beta^{(2)} + \ln\left(-\zeta_{\beta 0}^{(2)}\right)\left[\mathbf{B}^{(2)}\mathbf{I}_\beta\mathbf{q}_2^\infty - \mathbf{B}^{(1)}\mathbf{I}_\beta\mathbf{q}_1^\infty\right]\right\},$$

$$\mathbf{y}_k = \mathbf{B}^{(2)}\left\langle\left(\tau_{\alpha 0}^{(2)}\right)^k\right\rangle\mathbf{q}_2^\infty + \sum_{\beta=1}^{4}\mathbf{B}^{(2)}\left\langle\left(\hat{\tau}_{\alpha\beta}^{(2)}\right)^k\right\rangle\left(\mathbf{q}_\beta^{(2)} - \mathbf{I}_\beta\mathbf{q}_2^\infty\right),$$

$$\tau_{\alpha 0}^{(2)} = t_\alpha^{(2)}\zeta_{\alpha 0}^{(2)^{-1}}, \quad \hat{\tau}_{\alpha\beta}^{(2)} = t_\alpha^{(2)}\overline{\zeta}_{\beta 0}^{(2)}.$$

References

Barnett, D.M., Lothe, J., 1975. Dislocations and line charges in anisotropic piezoelectric insulators. Phys. Status Solidi. B 67, 105–111.

Barnett, D.M., Lothe, J., 1996. "Mutual" attraction of a dislocation to a bimetallic interface and a theorem on "proportional" anisotropic bimetals. Int. J. Solids Struct. 32, 291–301.

Chung, M.Y., Ting, T.C.T., 1996. Piezoelectric solid with an elliptic inclusion or hole. Int. J. Solids Struct. 33, 3343–3461.

Deeg, W.F., 1980. The analysis of dislocation, crack and inclusion problems in piezoelectric solids. Ph.D. Thesis. Stanford University, CA.

Deng, W., Meguid, S.A., 1998. Electro-elastic interaction between a screw dislocation and an elliptical inhomogeneity in piezoelectric materials. Int. J. Solids Struct. 35, 1467–1482.

Deng, W., Meguid, S.A., 1999. Analysis of a screw dislocation inside an elliptical inhomogeneity in piezoelectric solids. Int. J. Solids Struct. 36, 1449–1469.

Dundurs, J., Gangaharan, A.C., 1969. Edge dislocation near an inclusion with a slipping interface. J. Mech. Phys. Solids 17, 459–471.

Dundurs, J., Mura, T., 1964. Interaction between an edge dislocation and a circular inclusion. J. Mech. Phys. Solids 12, 177–189.

Dunn, M.L., Taya, M., 1993. An analysis of piezoelectric composite materials containing ellipsoidal inhomogeneities. Proc. Roy. Soc. Lond. A 443, 265–287.

Eshelby, J.D., 1956. The continuum theory of lattice defects. Solid State Physics 3, 79–144.

Hwu, C., Yen, W.J., 1993. On the anisotropic elastic inclusions in plane elastostatics. ASME J. Appl. Mech. 60, 626–632.

Kuang, Z.-B., Ma, F., 2001. Fields Near Crack Tip. Xi'an Jiaotong University Press, Xi'an.

Kuo, W.-S., Huang, J.-H., 1997. On the effective electroelastic properties of piezoelectric composites containing spatially oriented inclusions. Int. J. Solids Struct. 34, 2445–2461.

Liang, Y.C., Hwu, C., 1996. Electromechanical analysis of defects in piezoelectric materials, Smart. Mater. Struct. 5, 314–320.

Liu, J.X., Wang, B., Du, S.Y., 1997. Line force, charge and dislocation in anisotropic piezoelectric materials with an elliptic hole or a crack. Mech. Res. Commun. 24, 399–405.

Lu, P., Williams, F.W., 1998. Green functions of piezoelectric material with an elliptic hole or inclusion. Int. J. Solids Struct. 35, 651–664.

Pak, Y.E., 1990. Force on a piezoelectric screw dislocation. ASME J. Appl. Mech. 57, 863–869.

Pak, Y.E., 1992. Linear electro-elastic fracture mechanics of piezoelectric materials. Int. J. Fracture 54, 79–100.

Santare, M.H., Keer, L.M., 1986. Interaction between an edge dislocation and a rigid elliptical inclusion. ASME J. Appl. Mech. 53, 382–384.

Sosa, H.A., 1991. Plane problems in piezoelectric media with defects. Int. J. Solids Struct. 28, 491–505.

Sosa, H.A., Khutoryansky, N., 1996. New developments concerning piezoelectric materials with defects. Int. J. Solids Struct. 33, 3399–3414.

Stagni, L., 1995. Line singularity inside an elliptical inhomogeneity. Z. Angew. Math. Phys. 46, 630–634.

Stagni, L., 1999. The effect of the interface on the interaction of an interior edge dislocation with an elliptical inhomogeneity. Z. Angew. Math. Phys. 50, 327–337.

Suo, Z., Kuo, C.M., Barnett, D.M., Willis, J.R., 1992. Fracture mechanics for piezoelectric ceramics. J. Mech. Phys. Solids 40, 739–765.

Ting, T.C.T., 1996a. Green function for an anisotropic elliptic inclusion under generalized plane strain deformations. Quart. J. Mech. Appl. Math. 49, 1–17.

Ting, T.C.T., 1996b. Anisotropic Elasticity and it's application. Oxford University Press, London.

Wang, B., 1992. Three dimensional analysis of an ellipsoidal inclusion in piezoelectric material. Int. J. Solids Struct. 22, 965–983.

Warren, E.W., 1983. The edge dislocation inside an elliptical inclusion. Mech. Mater. 2, 319–330.
Yen, W.J., Hwu, C., 1994. Interactions between dislocations and anisotropic elastic elliptical inclusions. ASME J. Appl. Mech. 61, 548–554.
Yen, W.J., Hwu, C., Liang, Y.K., 1995. Dislocation inside, outside, or on the interface of an anisotropic elliptical inclusion. ASME J. Appl. Mech. 62, 306–311.